JOURNAL OF THE KOREAN ASTRONOMICAL SOCIETY
39: 31 ~ 40, 2006

SURVEY OF CARBON MONOXIDE OUTFLOWS ASSOCIATED WITH MOLECULAR HYDROGEN EMISSION FEATURES IN THE NORTHERN ORION A MOLECULAR CLOUD

GEUMSOOK PARK[1,2] AND MINHO CHOI[1]
[1] International Center for Astrophysics, Korea Astronomy and Space Science Institute, Daejeon 305-348
E-mail: pgs@kasi.re.kr & minho@kasi.re.kr
[2] Department of Astronomy and Space Science, Chungnam National University, Daejeon 305-764
(Received April 12, 2006; Accepted May 22, 2006)

ABSTRACT

Near-IR H_2 emission features in the northern region of the Orion A giant molecular cloud were observed in the CO $J = 1 \rightarrow 0$ line in search of CO outflows. Out of the 30 sources surveyed, CO line wings were detected toward 28 positions, suggesting a strong correlation between H_2 jets and CO outflows. Blueshifted wings were detected toward 26 positions while redshifted wings were detected toward 15 positions, which suggests that there is a bias in the source selection. The bias is more severe in OMC 3 than in OMC 2. Since the protostars in OMC 3 are younger and more deeply embedded, the bias may be caused by the difference of extinction between blueshifted and redshifted outflows. Some physical parameters of the outflows were derived from the line profiles.

Key words : ISM: individual (Orion A) — ISM: jets and outflows — stars: formation

I. INTRODUCTION

The outflow phenomenon of young stellar objects is one of the most important and easily noticeable star formation activities (Lada 1985). Primary outflows are probably in the form of neutral atomic gas (Natta et al. 1988; Lizano et al. 1988), and shocked regions can be observed in the optical band as Herbig-Haro objects and jets (Bachiller 1996; Richer et al. 2000; Reipurth & Bally 2001). Molecular outflows are mostly, if not entirely, ambient molecular medium swept up by the primary jet, and they are usually observed in molecular lines in the radio band, such as CO rotational transitions (Cabrit et al. 1997). Young stellar objects in the early stage of evolution are deeply embedded in molecular clouds, and their outflows are usually studied better with radio observations than with optical observations because of the huge extinction through the dense core around the driving source.

The shocked molecular gas at the shear zone or interface between the primary jet and the ambient molecular cloud can be traced by a number of shock tracers, such as the infrared (IR) lines of molecular hydrogen and the radio lines of SiO. The near-IR H_2 lines are good tracers of outflows driven by deeply embedded young stellar objects because they are less affected by the extinction than optical lines such as Hα. A good example is HH 211, which was found serendipitously during H_2 line observations of the IC 348 region (McCaughrean et al. 1994). Compared with the outflow tracers in the radio band, the H_2 lines can still be affected by foreground absorption and are less useful in studying the kinematics of outflow. Therefore, studies using the near-IR H_2 lines and the radio lines are complementary to each other.

Recent development of IR observation technology made it possible to survey a large region of the sky in search of molecular outflows using lines such as the 2.1 μm H_2 1–0 $S(1)$ line. Numerous H_2 emission features were detected in an unbiased survey of the Orion A giant molecular cloud (Stanke et al. 2002). Many of them were newly discovered outflows, and some of them were associated with thermal radio jets (Reipurth et al. 1999). This study provided a large sample of molecular outflows in a single giant molecular cloud, and the sample may be free from selection effects and contains sources located at roughly the same distance.

We observed the H_2 emission features detected by Stanke et al. (2002) in the CO $J = 1 \rightarrow 0$ line to study the outflow properties that are not available from the H_2 observations, such as the velocity structure and the mass of the outflowing molecular gas. Comparison between H_2 and CO is also interesting because the two tracers have very different cooling times (Eislöffel et al. 2000). The observations were made using the Taeduk Radio Astronomy Observatory (TRAO) 14 m telescope. We originally planned to cover all the H_2 features of Stanke et al. (2002), but this paper will present the results of observations of a subset of the whole sample. The reason for reporting the initial results before completing the survey is that TRAO is going through a major upgrade of observing instruments, including the installation of a multi-beam receiver system. As a consequence of the hardware upgrade, the data taken after the upgrade will be very different from the data obtained previously with a single receiver system, both

Corresponding Author: G. Park

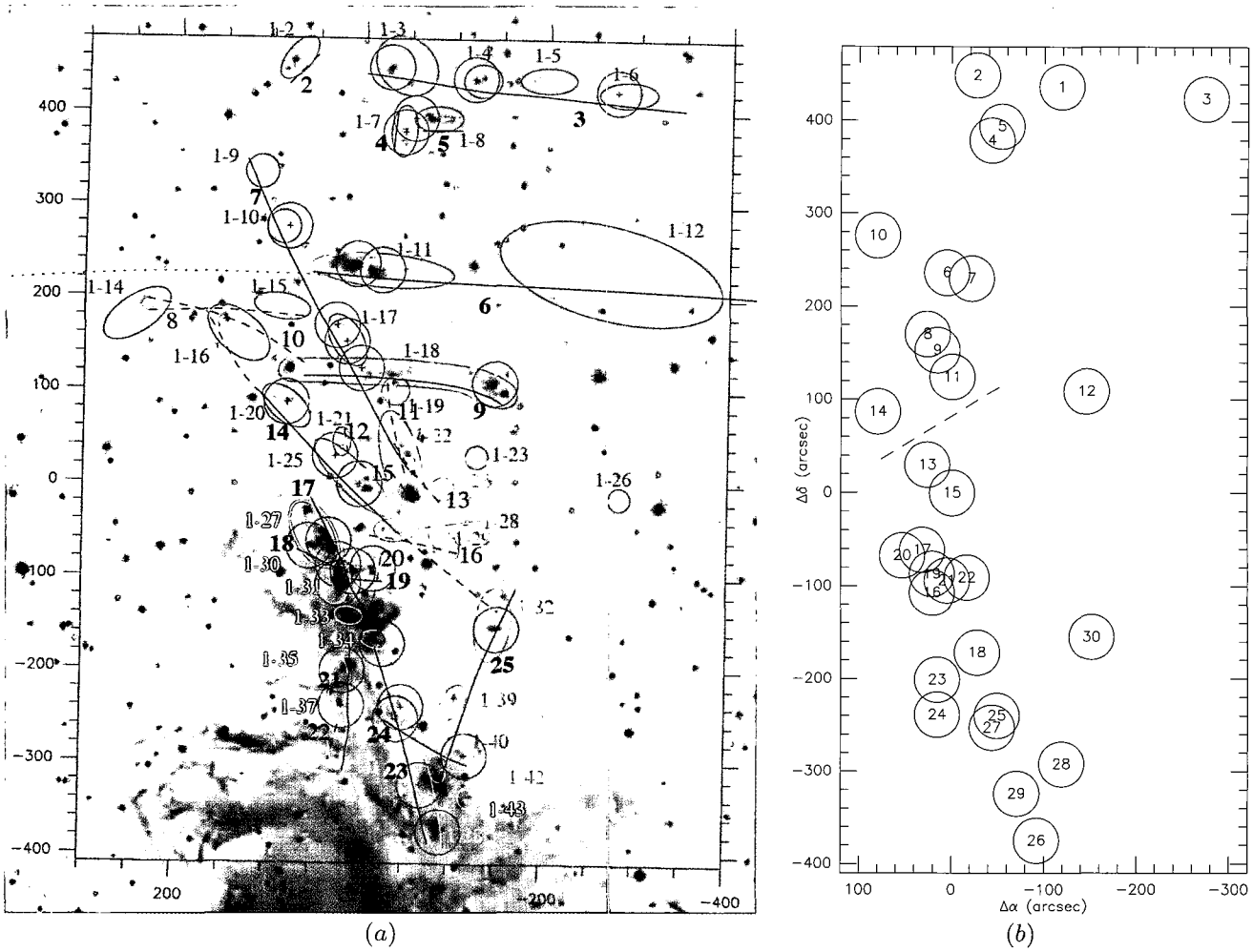

Fig. 1.— (*a*) CO source positions superposed on an H_2 image [Fig. 12 of Stanke et al. (2002)]. The axes are labeled in arcseconds. *Red circles*: Target CO source positions. Size of the circles corresponds to the beam size (FWHM). *Bluegreen or white ovals*: The H_2 features identified by Stanke et al. (2002). *Black lines*: The H_2 outflows identified by Stanke et al. (2002). (*b*) CO source positions labeled. *Dashed line*: Boundary between OMC 3 (to the north) and OMC 2 (to the south).

qualitatively and quantitatively. Therefore, instead of presenting an inhomogeneous set of data in a single paper, we decided to present the data obtained so far in this paper. We plan to continue our survey using the upgraded TRAO system in the future.

In this paper, we present our observations in the CO line toward the H_2 emission features in the northern region of Orion A. In Section II we describe our observations. In Section III we report the results of the CO line observations. In Section IV we describe the analysis of each spectrum and the outflow parameters. In Section V we discuss the implications of our results. A summary is given in Section VI.

II. OBSERVATIONS

(a) Source Selection

Stanke et al. (2002) divided their Orion A cloud H_2 survey area into several fields, and all the sources presented in this paper belong to Field 1, the northernmost field (Fig. 1). This region includes the well-known OMC 2/3. Stanke et al. (2002) identified 43 groups of H_2 features in Field 1, and each of them was named using the SMZ prefix. Structures larger than each SMZ sources were defined as jets and outflows on morphological grounds, and a total of 25 flows were identified in Field 1. Stanke et al. (2002) divided the flows into two groups. The "certain" group includes flows regarded as secure identifications, and the "uncertain" group includes insecurely identified flows consisting of

TABLE 1.
LIST OF SOURCES

SOURCE	FLOW[a]	OBJECT[b]	POSITION α_{2000}	POSITION δ_{2000}	NOISE (K)	ASSOCIATED OBJECTS
1.....	3	CRW MMS2	05 35 18.2	−05 00 33	0.5	VLA 1
2.....	3	SMZ 1-3A	05 35 24.4	−05 00 21	0.3	
3.....	3	SMZ 1-6A	05 35 07.8	−05 00 46	0.5	
4.....	4	CRW MMS6	05 35 23.3	−05 01 31	0.3	VLA 3
5.....	5	CRW MMS5	05 35 22.6	−05 01 16	0.4	
6.....	6	CRW MMS7	05 35 26.5	−05 03 54	0.6	VLA 4
7.....	6	SMZ 1-11A	05 35 24.7	−05 04 00	0.5	
8.....	7	SMZ 1-17A	05 35 28.0	−05 05 00	0.5	
9[c]....	7	SMZ 1-17B	05 35 27.2	−05 05 17	0.5	
10.....	7	SMZ 1-10	05 35 31.6	−05 03 14	0.3	
11.....	9	CRW MMS9	05 35 26.2	−05 05 46	0.2	VLA 5
12.....	9	SMZ 1-18B	05 35 16.4	−05 06 01	0.3	
13.....	14	CDS	05 35 28.0	−05 07 20	0.5	
14.....	14	SMZ 1-20A	05 35 31.6	−05 06 23	0.5	
15.....	14	SMZ 1-25A	05 35 26.2	−05 07 50	0.6	VLA 9
16.....	17	CRW FIR3	05 35 27.6	−05 09 37	0.6	VLA 11
17[d]....	17	SMZ 1-27C	05 35 28.3	−05 08 51	0.7	
18.....	17	SMZ 1-34A	05 35 24.4	−05 10 42	0.7	VLA 13
19.....	18	CDS	05 35 27.6	−05 09 17	0.7	
20[d]....	18	SMZ 1-27B	05 35 29.8	−05 08 57	0.5	
21.....	19	CDS	05 35 26.5	−05 09 24	0.6	
22.....	19	SMZ 1-30A	05 35 25.1	−05 09 21	0.6	
23.....	21	SMZ 1-37E	05 35 27.2	−05 11 11	0.5	
24.....	21	SMZ 1-37A	05 35 27.2	−05 11 49	0.5	
25.....	23	CDS	05 35 22.9	−05 11 50	0.4	
26.....	23	SMZ 1-38A	05 35 20.0	−05 14 05	0.6	
27.....	24	CDS	05 35 23.3	−05 12 03	0.5	
28.....	24	SMZ 1-40B	05 35 18.2	−05 12 42	0.5	
29.....	25	CRW FIR6c	05 35 21.5	−05 13 14	0.9	
30[e]....	25	SMZ 1-32A	05 35 16.1	−05 10 25	1.8	

NOTE.—Units of right ascension are hours, minutes, and seconds, and units of declination are degrees, arcminutes, and arcseconds. CRW source names are from Chini et al. (1997). VLA source numbers are from Reipurth et al. (1999).

[a] Flow number from Table 3 of Stanke et al. (2002).

[b] For the representative positions of "certain" flows, candidate driving sources (CDS) are listed. See Section 5.2 of Stanke et al. (2002) for details. For the other sources, the H_2 feature numbers from Table 2 of Stanke et al. (2002) are listed with the SMZ prefix.

[c] We originally planned to observe SMZ 1-18H. The coordinate of SMZ 1-18H, however, is listed incorrectly in Stanke et al. (2002). The observed source corresponds to SMZ 1-17B.

[d] Sources 17 and 20 include both SMZ 1-27B and SMZ 1-27C within the beam.

[e] SMZ 1-32A may belong to either flow 14 or flow 25.

poorly constraining H_2 features. We restricted our target sources to the certain flows.

Table 1 lists the parameters of sources presented in this paper. For all the certain flows, observations were made toward the representative position of the flow listed in Table 3 of Stanke et al. (2002), which is typically the position of the candidate driving source. Many of them are protostars detected in millimeter continuum (Chini et al. 1997). For flows longer than the beam size, additional observations were made toward some bright H_2 knots located relatively far away from the representative position of the flow. In this paper, we will name each source by combining the flow number prefixed by 'F' and the object name. For example, sources 2, 4, and 13 in Table 1 may be referred to as F3 SMZ 1-3A, F4 CRW MMS6, and F14 CDS, respectively.

(b) TRAO Observations

The H_2 emission features were observed in the CO $J = 1 \rightarrow 0$ line at 115.2712 GHz using the TRAO 14 m telescope in 2004 February. The data were obtained using the 3 mm superconductor-insulator-superconductor receiver. The spectrometer consisted of a 256-channel filter bank with a spectral channel width of 250 kHz (0.65 km s^{-1}).

The 14 m telescope had a main beam efficiency of

$\eta = 0.41$ and a beam size of FWHM = 49″ at the frequency of the CO line (Roh & Jung 1999). The efficiency was checked by observing Orion KL after each tuning and comparing with a standard spectrum. The peak intensity of Orion KL was consistent within 5.4%. We will present our data in terms of $T_{\rm mb} = T_A^* / \eta$. Telescope pointing was checked by regularly observing Orion KL in the SiO $v = 1$ $J = 2 \rightarrow 1$ maser line and was good within ~15″.

The data were taken by position switching with the off position of $(\Delta\alpha, \Delta\delta) = (-2°, -1°)$. A typical system temperature was 800 K, and the on-source integration time was 4–6 minutes for most sources.

III. RESULTS

For each spectrum a first order baseline was removed. The baseline was determined in the $V_{\rm LSR}$ intervals of (–20, –5) and (25, 40) in km s^{-1}. Occasional bad channels were flagged out. The spectra were averaged at each position. The resulting RMS noise levels are listed in Table 1, and spectra are shown in Figure 2. F25 SMZ 1-32A has a larger RMS noise level than the others because the integration time was shorter. A typical RMS noise level is 0.5 K.

IV. ANALYSIS

In this section we describe how we decided whether CO outflows were detected or not. Several assumptions were made to analyze the spectra. If there is a detectable molecular outflow in the beam, the spectrum would show a line profile that is a combination of the line core from the ambient cloud and the line wing from the molecular outflow. To separate the line wing component from the line core, the line core was assumed to have a Gaussian profile. The line wing component can be separated by fitting the line core with a Gaussian profile and by subtracting the fit from the original spectrum. Two methods were tried to find best-fit Gaussian profiles.

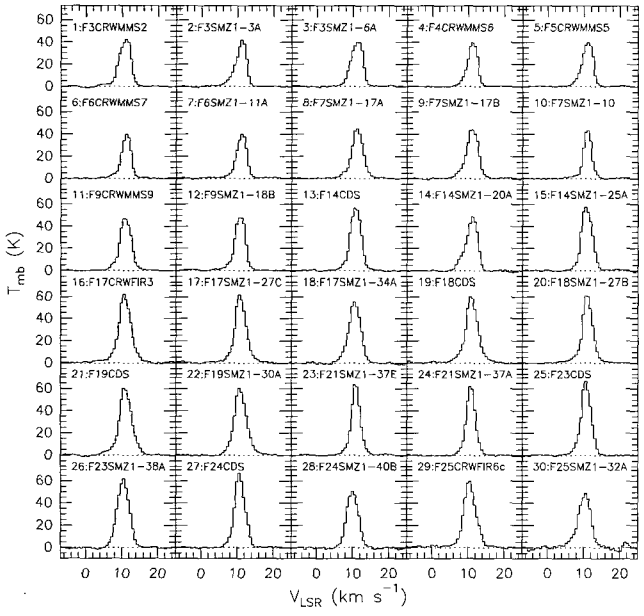

Fig. 2.— Spectra of the CO $J = 1 \rightarrow 0$ line toward the positions marked in Fig. 1. See Table 1 for the source names and parameters.

(a) Method I

The line core is assumed to be dominated by the emission from the ambient cloud. Free parameters of a Gaussian profile are $T_{\rm max}$, V_0, and FWHM, where $T_{\rm max}$ is the peak intensity, and V_0 is the central velocity. The fitting process was applied to the channels with intensities stronger than one-half of the maximum intensity. Typically 5 or 6 channels were used. The Gaussian profile is described by

$$T_{{\rm G},i} = T_{\rm max} \exp\left\{\frac{(V_i - V_0)^2}{{\rm FWHM}^2/4\ln 2}\right\}, \qquad (1)$$

where $T_{{\rm G},i}$ and V_i are the intensity and the velocity of each channel, respectively. A best-fit Gaussian profile

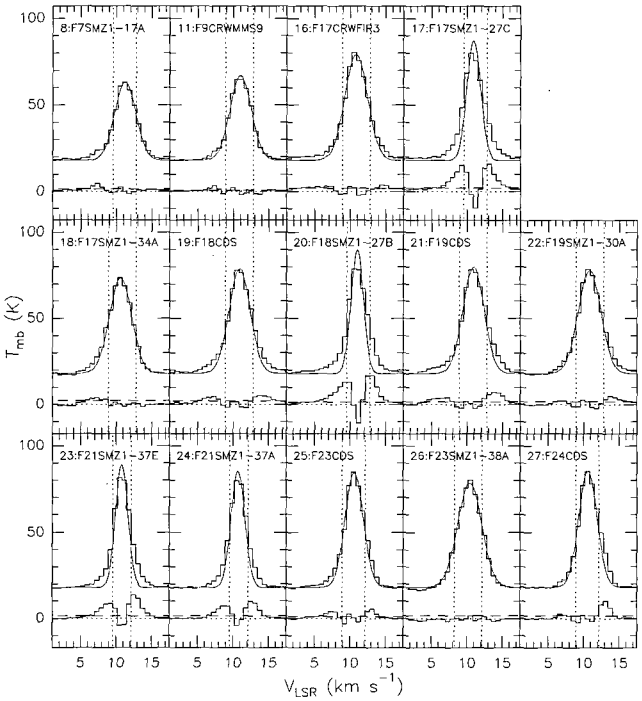

Fig. 3.— Spectra of the sources fitted with Method I only. In each panel, the upper histogram shows the observed spectrum, and the lower histogram shows the residual spectrum. *Red curves*: Gaussian profiles from Method I. *Vertical dotted lines*: Boundaries of the line core, showing the velocity interval considered in the Gaussian fitting process. *Horizontal dashed lines*: Intensity level at 3σ.

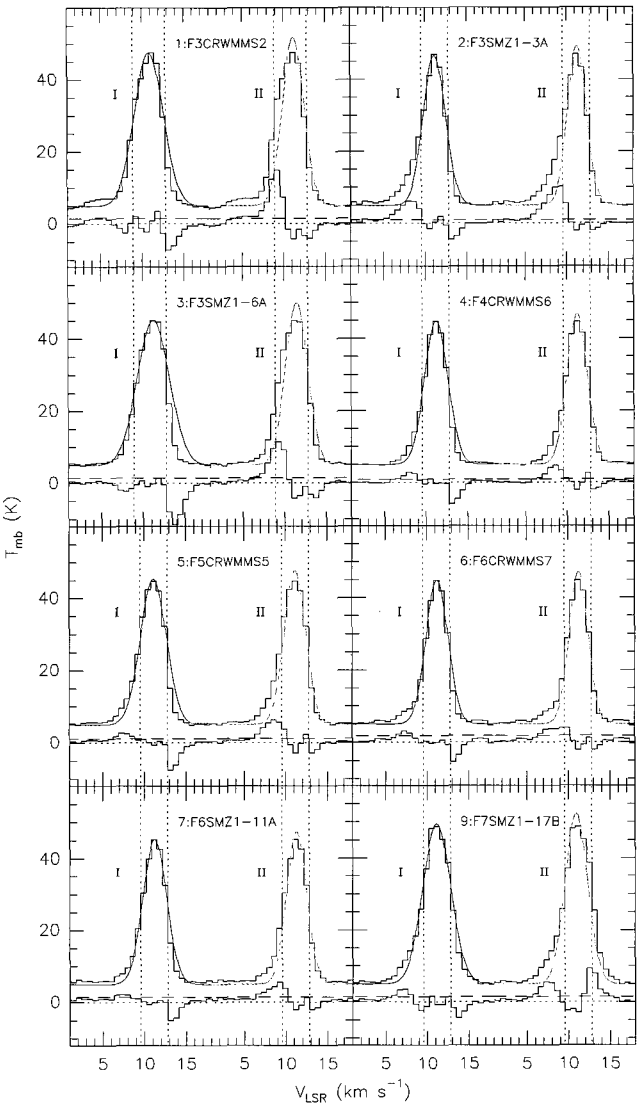

Fig. 4.— Spectra of the sources fitted with Methods I and II. The upper histograms show the observed spectra, and the lower histograms show the residual spectra. *Red curves*: Gaussian profiles from Method I. *Blue curves*: The Gaussian profiles from Method II. *Vertical dotted lines*: Boundaries of the line core, showing the velocity interval considered in the Gaussian fitting process. *Horizontal dashed lines*: Intensity level at 3σ.

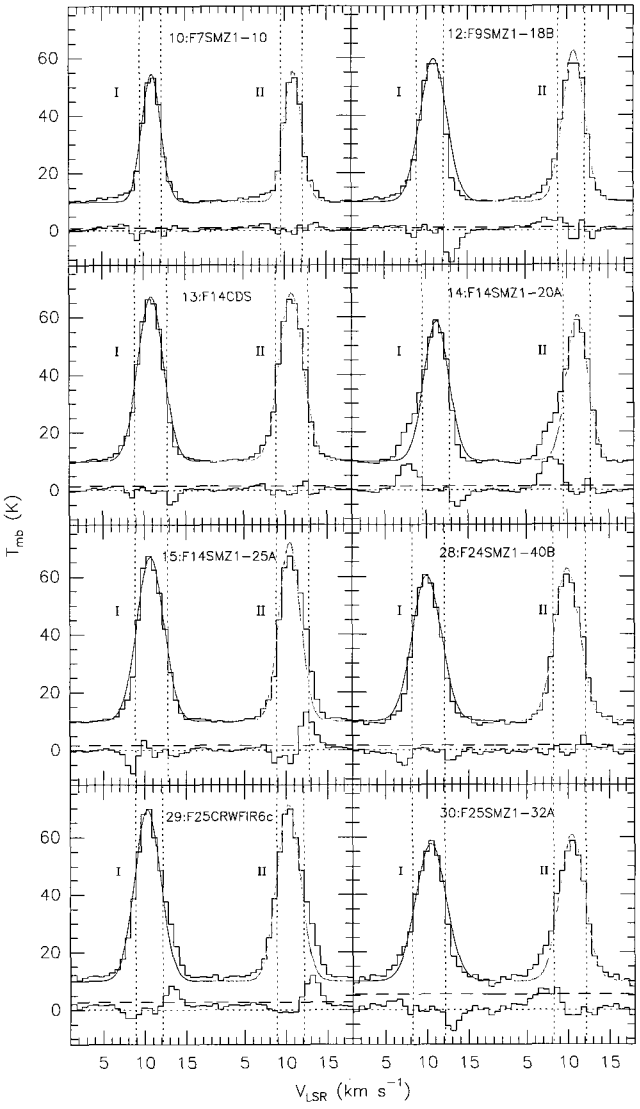

Fig. 5.— Spectra of the sources fitted with Methods I and II. See Fig. 4 for details.

was searched for by minimizing χ^2.

$$\chi^2 = \sum_i (T_{\mathrm{mb},i} - T_{\mathrm{G},i})^2/\sigma^2, \qquad (2)$$

where the summation is done over the velocity channels, and σ is the RMS noise. Figures 3–5 show the resulting fits, and Table 2 lists the best-fit parameters.

(b) Method II

When Method I was applied, some of the residual spectra showed channels with strong negative intensities located just outside the fitting interval. These negative channels can be caused by several reasons. (1) Bipolar outflows usually appear as two spatially separate lobes of emission, with one lobe mainly redshifted and the other mainly blueshifted (Lada 1985). If one of the two line wings is stronger than the other, the line profile can become highly asymmetric. The resulting residual spectra of Method I would show negative channels on the side with a weaker wing. (2) When the line core has a large optical depth, the line peak may be saturated, and the spectrum would show a non-Gaussian profile with a flat top. In this case, the residual spectrum would show negative channels on both sides.

TABLE 2.
GAUSSIAN FIT PARAMETERS

Source	Name	Method	V_0 (km s^{-1})	FWHM (km s^{-1})	T_{max} (K)
1....	F3 CRW MMS2	II	11.2	3.0	46.8
2....	F3 SMZ 1-3A	II	11.3	2.7	44.2
3....	F3 SMZ 1-6A	II	11.4	3.1	45.1
4....	F4 CRW MMS6	II	11.2	2.9	41.7
5....	F5 CRW MMS5	II	11.2	3.0	42.7
6....	F6 CRW MMS7	II	11.3	2.7	42.2
7....	F6 SMZ 1-11A	II	11.3	2.9	42.5
8....	F7 SMZ 1-17A	I	11.2	3.5	45.3
9....	F7 SMZ 1-17B	II	10.9	3.2	47.4
10....	F7 SMZ 1-10	II	10.9	2.5	45.5
11....	F9 CRW MMS9	I	11.0	3.5	48.9
12....	F9 SMZ 1-18B	II	10.8	3.1	52.5
13....	F14 CDS	II	10.7	3.4	58.5
14....	F14 SMZ 1-20A	II	11.2	3.0	50.5
15....	F14 SMZ 1-25A	II	10.5	3.0	61.9
16....	F17 CRW FIR3	I	10.8	3.8	61.2
17....	F17 SMZ 1-27C	I	10.9	2.3	69.3
18....	F17 SMZ 1-34A	I	10.6	3.7	55.5
19....	F18 CDS	I	10.9	3.5	60.7
20....	F18 SMZ 1-27B	I	11.0	2.0	72.1
21....	F19 CDS	I	10.9	3.5	61.8
22....	F19 SMZ 1-30A	I	10.8	3.8	59.9
23....	F21 SMZ 1-37E	I	10.8	2.0	71.3
24....	F21 SMZ 1-37A	I	10.7	2.3	67.4
25....	F23 CDS	I	10.6	3.0	66.5
26....	F23 SMZ 1-38A	I	10.4	4.0	60.6
27....	F24 CDS	I	10.6	3.0	67.5
28....	F24 SMZ 1-40B	II	9.9	3.6	52.6
29....	F25 CRW FIR6c	II	10.3	3.3	61.4
30....	F25 SMZ 1-32A	II	10.5	3.5	50.7

To handle such situations, an alternative method was used. First, V_0 was determined using the peak channel and the two adjacent channels. A parabolic fit was made to find V_0. Then the χ^2 fit was done by varying the T_{max} parameters. Initially a sufficiently large value of FWHM was tried, and progressively smaller values were tried. The iteration was finished when the minimum intensity channel of the residual spectrum is found inside the fitting interval, i.e., when the minimum channel in the line wing becomes similar to the minimum channel in the line core. This process would force the negative channels to become less severe. Figures 4 and 5 show the resulting fits from Method II. Table 2 lists the best-fit parameters.

Consistency between the two methods was checked using the spectra shown in Figure 3. In most cases, the fit parameters from Method II and those from Method I are similar within uncertainties. In some cases, the line wings (residuals) from Method II are weaker than those from Method I. Therefore, Method I finds line wings better than Method II, as long as it does not produce problematic negative channels in the residual spectrum.

For the 14 sources shown in Figure 3, only Method I was applied. For the others, both methods were applied, and the results of the Gaussian fit from Method II were used to derive physical parameters. Typical values of the Gaussian parameters are $V_0 \approx 11.1$ km s^{-1} and FWHM ≈ 3.4 km s^{-1}.

Over the whole region observed, V_0 shows a trend that the northern region is more redshifted than the southern region. The average V_0 of OMC 3 is 11.3 km s^{-1}, and the average V_0 of OMC 2 is 10.7 km s^{-1}. This velocity structure is consistent with the result of the CS mapping by Tatematsu et al. (1993). The distribution of FWHM does not show a clear trend.

V. DISCUSSION

(a) Statistics

Out of the 30 positions observed, twelve sources showed detectable line wings on both the blue and the red sides. The number of blue wings was larger than that of red wings: blue wings were detected toward 26 sources while red wings were detected toward 14 sources. Typical $|V_{blue} - V_0|$ was 5.8 km s^{-1} and typ-

ical $|V_{\rm red} - V_0|$ was 4.6 km s^{-1}. Two sources (sources 26 and 28) did not show line wings above 3σ limits.

Most flows were observed at multiple positions, and a total of 14 flows were observed. CO line wings were detected in all flows. Five flows show blue wings only. There is no flow showing red wing only. However, some areas are crowded with multiple flows (e.g., flows 17, 18, and 19). Though spectra of such areas show both blue and red wings, it is difficult to separate the contribution from each flow. Those flows showing only blue wings are located in relatively less crowded area.

The excess of blue wings suggests that there may be a bias in selecting the target positions. A possibility is that the extinction in the near-IR band may make the H_2 emissions from redshifted outflows appear weaker than those from blueshifted outflows, which can introduce a bias when the source selection was made based on bright H_2 features. Another possibility is that some driving sources are located near the surface of the molecular cloud on the far side. In such a configuration, there are little molecules around the redshifted outflow escaping the cloud, while the blueshifted outflow propagate through the dense molecular cloud.

Interestingly, there is a clear difference between OMC 2 and OMC 3. Among the 12 sources in OMC 3 (see Fig. 1*b*), 2 sources (17%) show both blue and red wings, most sources (83%) show blue wings only, and no source shows red wing only. In contrast, among the 18 sources in OMC 2, most sources (56%) show both wings, 4 sources (22%) show blue wings only, and 2 sources (11%) show red wings only. Submillimeter continuum studies showed that the protostars in OMC 3 are younger than those in OMC 2 (Chini et al. 1997). This age difference supports the idea that the excess of blue wings was caused by the difference of extinction between the blueshifted and the redshifted H_2 outflows. That is, the protostars in OMC 3 are deeply embedded, and most of the redshifted H_2 emission features may have been undetected because of the high extinction. This trend suggests that the H_2 line is a good indicator of outflow activity in clouds containing relatively evolved (Class I or higher) protostars, while it can miss many outflow activities of the youngest (Class 0) protostars. For such deeply embedded young protostars, other shock tracers in the radio wavelength (such as SiO lines) may be better indicators of outflow activity.

(b) Outflow Parameters

The column density of H_2 was calculated by

$$N_{\rm H_2} = 2.3 \times 10^{20} \int T_{\rm mb} dV, \quad (3)$$

where $N_{\rm H_2}$ is in units of cm^{-2}, and $\int T_{\rm mb} dV$ is the integrated intensity of the CO $J = 1 \rightarrow 0$ line in K km s^{-1} (Rohlfs & Wilson 2000). The integrated intensities are listed in Table 3. The mass in the outflowing gas can be calculated by

$$M = 1.3 m_{\rm H_2} N_{\rm H_2} A, \quad (4)$$

where $m_{\rm H_2}$ is the mass of a hydrogen molecule, $A = \pi({\rm FWHM}\ d/2)^2$ is the area, and d is the distance. The distance to the Orion A cloud is assumed to be 450 pc (Genzel & Stutzki 1989).

The momentum and the kinetic energy of each outflow were calculated by

$$P = M \frac{\int |V - V_0| T_{\rm mb} dV}{\int T_{\rm mb} dV}, \quad (5)$$

and

$$E_K = \frac{1}{2} M \frac{\int |V - V_0|^2 T_{\rm mb} dV}{\int T_{\rm mb} dV}, \quad (6)$$

The outflow parameters are listed in Table 4.

Our observation field was surveyed in the CO $J = 1 \rightarrow 0$ line by other investigators (Aso et al. 2000; Williams et al. 2003). They calculated the column density of H_2 with the assumption that the CO line is optically thin. We calculated the column density using empirical value of the conversion factor between CO integrated line intensity and mass (Rohlfs & Wilson 2000). Because of the difference in the assumptions about the optical depth, the masses listed in Table 4 are larger than the masses calculated by Aso et al. (2000) and Williams et al. (2003), typically by a factor of 10.

Masses of outflowing gas are typically 10–100 $M_\odot$ for high-mass protostars (Zhang et al. 2005), and those of low-mass protostars are typically 0.1–1 $M_\odot$ (for example, Goldsmith et al. 1984). The outflow masses in our survey are typically 1–3 $M_\odot$, suggesting that these outflows may be driven by low-mass protostars.

(c) Note on Individual Flows

This paper presents CO spectra of 14 flows observed at 30 positions. The shape of each flow determined by Stanke et al. (2002) is shown in Figure 1. Physical properties are listed in Tables 3 and 4. Short notes on some flows are listed below.

FLOW 3.—Three positions along this H_2 flow were observed. Blueshifted CO outflows were found, but no red wing was detected. The driving source, MMS 2, is associated with the centimeter continuum source VLA 1, probably a radio jet (Reipurth et al. 1999).

FLOWS 4/5.—Since the beam areas of sources 4 and 5 partly overlap (Fig. 1b), their CO spectra are not completely independent. The driving source of flow 4, MMS 6, is the brightest (sub)millimeter continuum source in this region and is associated with VLA 3 (Chini et al. 1997; Reipurth et al. 1999).

FLOW 6.—The driving source, MMS 7, is associated with IRAS 05329–0505 and VLA 4 (Reipurth et al. 1999). 5A

FLOW 9.—This is a relatively well-defined and long outflow. Only blue wings were detected. Since we only

TABLE 3.
WING PARAMETERS

SOURCE	NAME	V^{a}_{blue}	V^{a}_{red}	$\lvert V_{blue} - V_0 \rvert$	$\lvert V_{red} - V_0 \rvert$	$\int T_{mb} dV^{b}$ Blue	$\int T_{mb} dV^{b}$ Red
1.....	F3 CRW MMS2	3.7	...	7.5	...	34.6 ± 1.0	...
2.....	F3 SMZ 1-3A	2.4	...	8.9	...	31.5 ± 0.6	...
3.....	F3 SMZ 1-6A	6.3	...	5.1	...	25.9 ± 0.8	...
4.....	F4 CRW MMS6	5.7	...	5.5	...	11.3 ± 0.5	...
5.....	F5 CRW MMS5	5.7	...	5.5	...	18.6 ± 0.6	...
6.....	F6 CRW MMS7	6.3	...	5.0	...	13.8 ± 1.0	...
7.....	F6 SMZ 1-11A	6.3	...	5.0	...	14.6 ± 0.8	...
8.....	F7 SMZ 1-17A	6.3	...	4.9	...	6.6 ± 0.5	...
9.....	F7 SMZ 1-17B	5.7	15.4	5.2	4.5	13.2 ± 0.7	17.2 ± 0.8
10.....	F7 SMZ 1-10	4.3	14.7	6.6	3.8	6.2 ± 0.5	4.4 ± 0.4
11.....	F9 CRW MMS9	5.7	...	5.3	...	4.7 ± 0.3	...
12.....	F9 SMZ 1-18B	3.1	...	7.7	...	17.5 ± 0.7	...
13.....	F14 CDS	6.3	...	4.4	...	2.6 ± 0.5	...
14.....	F14 SMZ 1-20A	5.7	...	5.5	...	31.5 ± 0.8	...
15.....	F14 SMZ 1-25A	...	14.8	...	4.3	...	25.2 ± 0.8
16.....	F17 CRW FIR3	1.8	15.4	9.0	4.6	14.4 ± 1.2	7.6 ± 0.8
17.....	F17 SMZ 1-27C	5.0	16.0	5.9	5.1	37.5 ± 1.2	34.4 ± 1.1
18.....	F17 SMZ 1-34A	5.7	...	4.9	...	10.3 ± 1.1	...
19.....	F18 CDS	5.0	16.7	5.9	5.8	11.5 ± 1.0	15.7 ± 1.1
20.....	F18 SMZ 1-27B	3.1	16.0	7.9	5.0	38.0 ± 0.9	35.9 ± 0.8
21.....	F19 CDS	4.3	16.0	6.6	5.1	13.7 ± 1.0	20.0 ± 0.9
22.....	F19 SMZ 1-30A	6.3	16.7	4.5	5.9	3.0 ± 0.5	12.6 ± 0.9
23.....	F21 SMZ 1-37E	6.3	14.7	4.5	3.9	22.6 ± 0.8	27.5 ± 0.7
24.....	F21 SMZ 1-37A	6.3	14.7	4.4	4.0	18.4 ± 0.8	20.1 ± 0.7
25.....	F23 CDS	5.0	14.1	5.6	3.5	9.1 ± 0.6	8.1 ± 0.5
26.....	F23 SMZ 1-38A	...	...	...	...	...	...
27.....	F24 CDS	6.3	14.7	4.3	4.1	3.1 ± 0.5	16.8 ± 0.7
28.....	F24 SMZ 1-40B	...	...	...	...	...	...
29.....	F25 CRW FIR6c	...	14.7	...	4.4	...	25.9 ± 1.3
30.....	F25 SMZ 1-32A	6.3	...	4.2	...	9.2 ± 1.6	...

NOTE.—No data means no detectable wing. All velocities are in km s^{-1}.
[a] Wing boundaries where the intensity falls below the 3σ level.
[b] Integrated intensity in K km s^{-1}.

covered the driving source and the western outflow, it is not clear whether the eastern outflow is redshifted. The driving source, MMS 9, is associated with VLA 5 (Reipurth et al. 1999). Source 11 is located at the intersection between flows 7 and 9.

FLOW 14.—This is a good example showing highly collimated bipolar structure. The northeastern outflow shows a blue wing, and the southwestern outflow shows a red wing. Source 15 (SMZ 1-25A) is associated with VLA 9 (Reipurth et al. 1999), but it does not coincide with any of the millimeter continuum sources.

FLOWS 17–19.—Since flows 17, 18, and 19 are close to each other, their CO spectra are not completely independent. FIR 3 (source 16) is associated with VLA 11 (Reipurth et al. 1999). Source 18 (SMZ 1-34A) is associated with VLA 13, an extended centimeter continuum source elongated roughly in the direction of flow 17, which supports the interpretation that VLA 13 is a collimated radio jet (Reipurth et al. 1999).

FLOWS 23/24.—Source 18 is located at the intersection between flows 17 and 23. Since the beam areas of sources 25 and 27 partly overlap (Fig. 1b), their CO spectra are not completely independent.

VI. SUMMARY

We observed the northern region of the Orion A giant molecular cloud in the CO $J = 1 \rightarrow 0$ line. These positions were selected based on the H_2 features reported by Stanke et al. (2002). CO outflows were detected toward most of the positions surveyed, suggesting that there is a close relation between shocked H_2 emission features and CO molecular outflows, as expected from standard outflow models.

Out of the 30 positions observed, blue wings were detected toward 26 positions while red wings were detected toward 15 positions. Many flows were observed at multiple positions, and a total of 14 flows were observed. Nine flows show both blue and red wings while

TABLE 4.
OUTFLOW PARAMETERS

		N_{H_2} (10^{20} cm^{-2})		M ($M_\odot$)		P ($M_\odot$ km s^{-1})		E_K (10^{43} erg)	
SOURCE	NAME	Blue	Red	Blue	Red	Blue	Red	Blue	Red
1.....	F3 CRW MMS2	79.7	...	1.48	...	3.87	...	13.5	...
2.....	F3 SMZ 1-3A	72.4	...	1.35	...	4.19	...	16.1	...
3.....	F3 SMZ 1-6A	59.6	...	1.11	...	2.70	...	7.5	...
4.....	F4 CRW MMS6	26.1	...	0.48	...	1.48	...	5.0	...
5.....	F5 CRW MMS5	42.8	...	0.80	...	2.26	...	7.3	...
6.....	F6 CRW MMS7	31.7	...	0.59	...	1.68	...	5.5	...
7.....	F6 SMZ 1-11A	33.6	...	0.62	...	1.71	...	5.3	...
8.....	F7 SMZ 1-17A	15.2	...	0.28	...	1.13	...	4.6	...
9.....	F7 SMZ 1-17B	30.4	39.6	0.56	0.74	2.13	1.44	8.4	3.4
10.....	F7 SMZ 1-10	14.2	10.2	0.26	0.19	1.11	0.72	5.0	4.1
11.....	F9 CRW MMS9	10.8	...	0.20	...	0.79	...	3.2	...
12.....	F9 SMZ 1-18B	40.3	...	0.75	...	3.16	...	21.7	...
13.....	F14 CDS	6.0	...	0.11	...	0.43	...	1.7	...
14.....	F14 SMZ 1-20A	72.6	...	1.35	...	4.28	...	14.9	...
15.....	F14 SMZ 1-25A	...	57.9	...	1.08	...	2.23	...	5.2
16.....	F17 CRW FIR3	33.1	17.5	0.62	0.32	3.09	0.99	18.2	3.6
17.....	F17 SMZ 1-27C	86.2	79.1	1.60	1.47	3.82	3.82	11.2	11.2
18.....	F17 SMZ 1-34A	23.7	...	0.44	...	1.46	...	5.2	...
19.....	F18 CDS	26.5	36.1	0.49	0.67	2.05	2.39	8.9	9.2
20.....	F18 SMZ 1-27B	87.4	82.5	1.62	1.53	4.36	3.44	15.2	8.9
21.....	F19 CDS	31.6	46.1	0.59	0.86	2.54	2.64	12.2	8.9
22.....	F19 SMZ 1-30A	6.8	29.0	0.13	0.54	0.49	1.98	1.9	7.9
23.....	F21 SMZ 1-37E	51.9	63.3	0.96	1.18	2.15	2.39	5.6	5.5
24.....	F21 SMZ 1-37A	42.2	46.3	0.78	0.86	1.79	1.83	4.7	4.3
25.....	F23 CDS	20.9	18.6	0.39	0.35	1.41	0.84	5.4	2.1
26.....	F23 SMZ 1-38A	...	...	...	...	...	...	...	...
27.....	F24 CDS	7.2	38.7	0.13	0.72	0.49	1.83	1.8	4.9
28.....	F24 SMZ 1-40B	...	...	...	...	...	...	...	...
29.....	F25 CRW FIR6c	...	59.5	...	1.10	...	3.11	...	9.4
30.....	F25 SMZ 1-32A	21.2	...	0.39	...	1.37	...	4.8	...

five flows show blue wings only. These statistics suggest that source selection based on H_2 features could introduce a bias, which is probably owing to the extinction in the near-IR band. The bias is more severe in OMC 3 than in OMC 2, which may reflects the difference in the evolutionary stages of the protostars.

Some physical parameters of each outflow were derived. The outflow mass is typically comparable to one solar mass.

ACKNOWLEDGEMENTS

This work was partially supported by the Korea-Japan Basic Scientific Cooperation Program of KOSEF and by the LRG Program of KASI.

REFERENCES

Aso, Y., Tatematsu, K., Sekimoto, Y., Nakano, T., Umemoto, T. Koyama, K., & Yamamoto, S., 2000, Dense Cores and Molecular Outflows in the OMC-2/3 Region, ApJS, 131, 465

Bachiller, R., 1996, Bipolar Molecular Outflows from Young Stars and Protostars, ARA&A, 34, 111

Cabrit, S., Raga, A., & Gueth, F., 1997, in IAU Symp. 182, Herbig-Haro Flows and the Birth of Stars, ed. B. Reipurth & C. Bertout (Dordrecht: Kluwer), 163

Chini, R., Reipurth, B., Ward-Thompson, D., Bally, J., Nyman, L.-Å., Sievers, A., & Billawala, Y., 1997, Dust Filaments and Star Formation in OMC-2 and OMC-3, ApJ, 474, L135 (CRW)

Eislöffel, J., Mundt, R., Ray, T. P., & Rodríguez, L. F., 2000, in Protostars and Planets IV, ed. V. Mannings, A. P. Boss, & S. S., Russell (Tucson: Univ. of Arizona Press), 815

Genzel, R. & Stutzki, J., 1989, The Orion Molecular Cloud and Star-forming Region, ARA&A, 27, 41

Goldsmith, P. F., Snell, R. L., & Hemeon-Heyer M., 1984, Bipolar Outflows in Dark Clouds, ApJ, 286, 599

Lada, C. J., 1985, Old Outflows, Energetic Winds, and Enigmatic Jets around Young Stellar Objects, ARA&A, 23, 267

Lizano, S., Heiles, C., Rodríguez, L. F., Koo, B. C., Shu, F. H., Hasegawa, T., & Hayashi, S., 1988, Neutral Stellar Winds that Drive Bipolar Outflows in Low-mass Protostars, ApJ, 328, 763

McCaughrean, M. J., Rayner, J. T., & Zinnecker, H., 1994, Discovery of a Molecular Hydrogen Jet near IC 348, ApJ, 436, L189

Natta, A., Giovanardi, C., & Palla, F., 1988, Neutral Winds from Cool Young Stars - A Solution to the Line Deficit Problem, ApJ, 327, 817

Reipurth, B., Rodríguez, L. F., & Chini, R., 1999, VLA Detection of Protostars in OMC-2/3, AJ, 118, 983

Reipurth, B. & Bally, J., 2001, Herbig-Haro Flows: Probes of Early Stellar Evolution, ARA&A, 39, 403

Richer, J. S., Shepherd, D. S., Cabrit, S., Bachiller, R., & Churchwell, E., 2000, in Protostars and Planets IV, ed. V. Mannings, A. P. Boss, & S. S. Russell (Tucson: Univ. of Arizona Press), 867

Roh, D.-G. & Jung, J. H., 1999, Characteristics of TRAO 14m Radio Telescope (1999), PKAS, 14, 123

Rohlfs, K. & Wilson, T. L., 2000, Tools of Radio Astronomy, (Berlin: Springer)

Stanke, T., McCaughrean, M. J., & Zinnecker, H., 2002, An Unbiased H_2 Survey for Protostellar Jets in Orion A. II. The Infrared Survey Data, A&A, 392, 239 (SMZ)

Tatematsu, K., et al., 1993, Molecular Cloud Cores in the Orion A Cloud. I - Nobeyama CS (1-0) Survey, ApJ, 404, 643

Williams, J. P., Plambeck, R. L., & Heyer, M. H., 2003, High-Resolution Imaging of CO Outflows in OMC-2 and OMC-3, ApJ, 591, 1025

Zhang, Q., Hunter, T. R., Brand J., Sridharan, T. K., Cesaroni, R., Molinari S., Wang, J., & Kramer M., 2005, Search for CO Outflows toward a Sample of 69 High-Mass Protostellar Candidates. II. Outflow Properties, ApJ, 625, 864